JOURNAL OF SOLID STATE CHEMISTRY 117, 127–135 (1995)

The Reduction Behavior of Fe–Mo–O Catalysts Studied by Temperature-Programmed Reduction Combined with *in Situ* Mössbauer Spectroscopy and X-Ray Diffraction

Huiliang Zhang,[1] Jianyi Shen, and Xin Ge

Department of Chemistry, Nanjing University, Nanjing, 210093, China

Received August 1, 1994; accepted November 22, 1994

The reduction processes of Fe–Mo–O catalysts with different Fe/Mo atomic ratios were studied by means of temperature-programmed reduction (TPR). In particular, the reduction process of a sample with an Fe/Mo ratio of 0.29 was investigated in detail in combination with *in situ* Mössbauer spectroscopy (MBS) and X-ray diffraction (XRD). Five peaks are observed in the TPR profile of this sample with peak temperatures at 853, 910, 952, 1014, and 1233 K, respectively, indicating that the reduction of the catalyst proceeds via five stages. MBS and XRD showed that the phases in the sample are MoO_3 and $Fe_2(MoO_4)_3$ before TPR. At the first TPR peak (853 K), $Fe_2(MoO_4)_3$ was completely transformed into β-$FeMoO_4$ and Mo_4O_{11}, while MoO_3 was not affected. The β-$FeMoO_4$ phase that formed can convert to α-$FeMoO_4$ when the reduced sample is exposed to air at room temperature. The second TPR peak (910 K) corresponds to the reduction of MoO_3 to MoO_2. At the third TPR peak (952 K), Mo_4O_{11} was reduced to MoO_2 and most of the β-$FeMoO_4$ was transformed to $Fe_2Mo_3O_8$ and Fe_3O_4. The Mössbauer spectrum of $FeMo_3O_8$ can be fitted with two doublets (IS = 0.90 mm/sec, QS = 0.58 mm/sec and IS = 1.03 mm/sec, QS = 1.05 mm/sec). It is interesting to note that at this stage some Fe^{2+} ions were reoxidized to Fe^{3+}, and Fe_3O_4 is formed, probably due to the reaction between Mo^{6+} and Fe^{2+} in β-$FeMoO_4$. At the fourth TPR peak (1014 K), β-$FeMoO_4$ was completely converted and the Fe–Mo alloy (a singlet in the Mössbauer spectrum with IS = −0.21 mm/sec) was formed, resulting from the reduction of MoO_2 and Fe_3O_4 or $Fe_2Mo_3O_8$. At the last peak (1233 K), all the metal oxides (MoO_2 and Fe_3O_4 or $Fe_2Mo_3O_8$) were reduced to metals. The products detected are Fe_3Mo alloy and metallic molybdenum.

INTRODUCTION

Iron–molybdenum mixed oxide is the main component of catalysts for the partial oxidation of alcohols and hydrocarbons. For example, it has been used for the production of formaldehyde from methanol on a commercial scale (1, 2). Boreskov *et al.* (3) and Okamoto *et al.* (4) showed that the excess of MoO_3 in Fe–Mo–O catalysts promoted the formation of stoichiometric ferric molybdate, which is the active phase for the oxidation of methanol to formaldehyde. Germain *et al.* (5) showed that Fe–Mo–O catalysts exhibited good catalytic activity for the oxidation of toluene to benzaldehyde. In previous papers (6, 7), we have reported that the composition and structure of Fe–Mo–O catalysts strongly influenced the selective oxidation of toluene to benzaldehyde and that the catalyst with an Fe/Mo atomic ratio of 0.29 exhibited the highest activity and selectivity. Trifiro *et al.* (8) studied the reduction of Fe–Mo–O catalysts in NH_3/N_2 and H_2/N_2 and found that MoO_3 and $Fe_2(MoO_4)_3$ in the catalysts can be reduced to MoO_2 and $FeMoO_4$, respectively, and that the latter was then reoxidized to $Fe_2(MoO_4)_3$ by O_2. Carbucicchio *et al.* (9) observed by Mössbauer spectroscopy that $Fe_2(MoO_4)_3$ was reduced to β-$FeMoO_4$ when treated in CH_3OH/N_2. We also found (10) that $Fe_2(MoO_4)_3$ was converted to β-$FeMoO_4$ when Fe–Mo–O catalysts were used for the oxidation of toluene to benzaldehyde and that the activity of the catalysts was related to the amount of β-$FeMoO_4$ formed. Gai *et al.* (11) studied Fe–Mo–O catalysts using electron microscopy in an atmosphere of methanol, methanol/oxygen, or hydrogen. They declared that the reduction of the catalysts proceeded via two or possibly three reaction routes simultaneously. Having used *in situ* Raman spectroscopy to study supported and unsupported Fe–Mo–O catalysts, Hill *et al.* (12) reported that the band intensities in Raman spectra were related to the reduction extent of catalysts: fully oxidized catalysts were stronger Raman scatterers than partially reduced catalysts. In those experiments, the Raman spectra of the Fe–Mo–O catalysts were collected during *in situ* methanol oxidation to formaldehyde. An XPS study of the Fe–Mo catalyst (13) during reduction with H_2 indicated that Mo^{6+} ions on the sample surface were reduced to Mo^{5+} and Mo^{4+}, and then were reoxidized to Mo^{6+} by

[1] To whom correspondence should be addressed.

0022-4596/95 $6.00

Fe^{3+}. The Fe^{3+} ions were reduced to Fe^{2+}, due to the interactions with Mo^{5+} and Mo^{4+} ions, and then were reduced by H_2.

Because of the importance of the reduction behavior of Fe–Mo–O catalysts in relation to their catalytic reactivity for partial oxidation reactions, we used temperature-programmed reduction (TPR) to study the reduction processes of Fe–Mo–O catalysts. In particular, a sample with an Fe/Mo ratio of 0.29 was studied in detail in combination with *in situ* Mössbauer spectroscopy (MBS) and X-ray diffraction (XRD) to monitor the phase changes at different reduction stages.

EXPERIMENTAL

The aqueous solution of ferric nitrate was added into the aqueous solution of ammonium molybdate at about 313 K under stirring. The pH of the mixture was maintained at 4–5 by the addition of NH_4OH. The precipitate formed was dried in a circulating film-evaporator and was calcined at 773 K for 8 hr. The sample obtained was then pelleted, crushed, and sieved.

The TPR apparatus used in this work is similar to that described in (14). About 20 mg of sample was loaded in a quartz U-tube. A mixture of N_2 and H_2 (7.63% H_2) with purity 99.999% was used, and the flow rate was maintained at 20 ml/min. The temperature was raised at a programmed rate of 10 K/min from room temperature to around 1373 K. The amount of hydrogen consumed for each peak in the TPR profile was obtained from the peak areas with a normalization method.

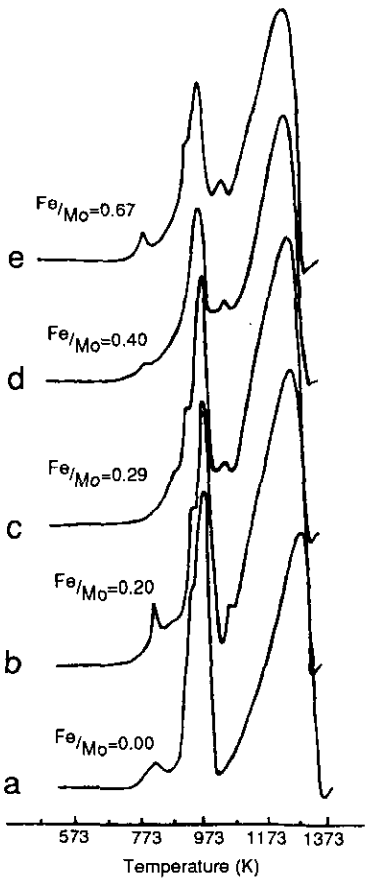

FIG. 1. TPR profiles of Fe–Mo–O catalysts with different Fe/Mo atomic ratios as indicated.

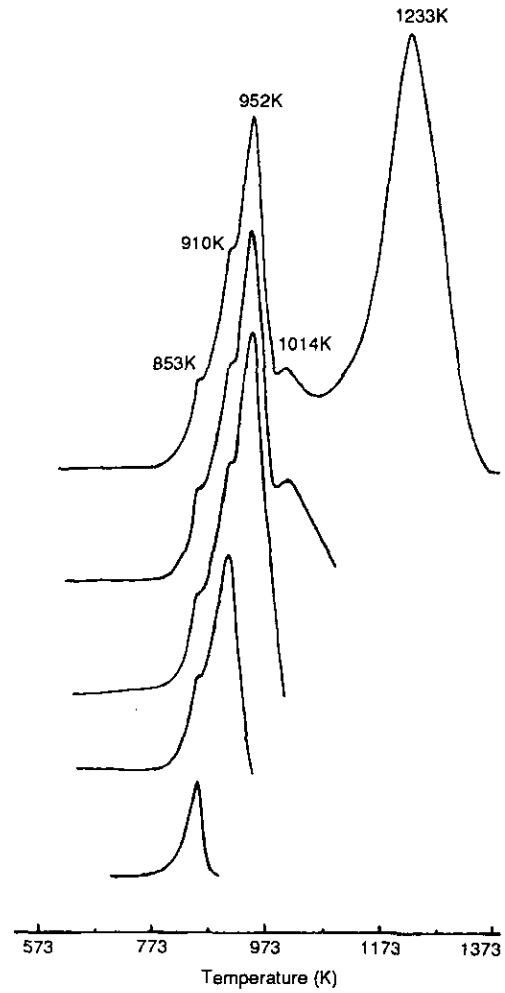

FIG. 2. TPR profiles of the Fe–Mo–O catalyst with an Fe/Mo atomic ratio of 0.29 at different reduction stages.

To collect Mössbauer spectra without exposing the sample to air after each TPR peak, an *in situ* quartz cell was adopted as described in Ref. (15). About 100 mg of the sample was used in order to obtain good Mössbauer spectra. For each TPR peak, the temperature was raised to the peak position and maintained until the peak was complete. The sample was then cooled to room temperature in flowing N_2–H_2 and sealed for Mössbauer determination. The Mössbauer spectra were recorded using a 15 mCi ^{57}Co (Pd) source on a constant acceleration spectrometer. The spectra were computer-fitted to the Lorentzian lines by a least-squares program. The velocity of the spectrometer was calibrated with respect to α-Fe.

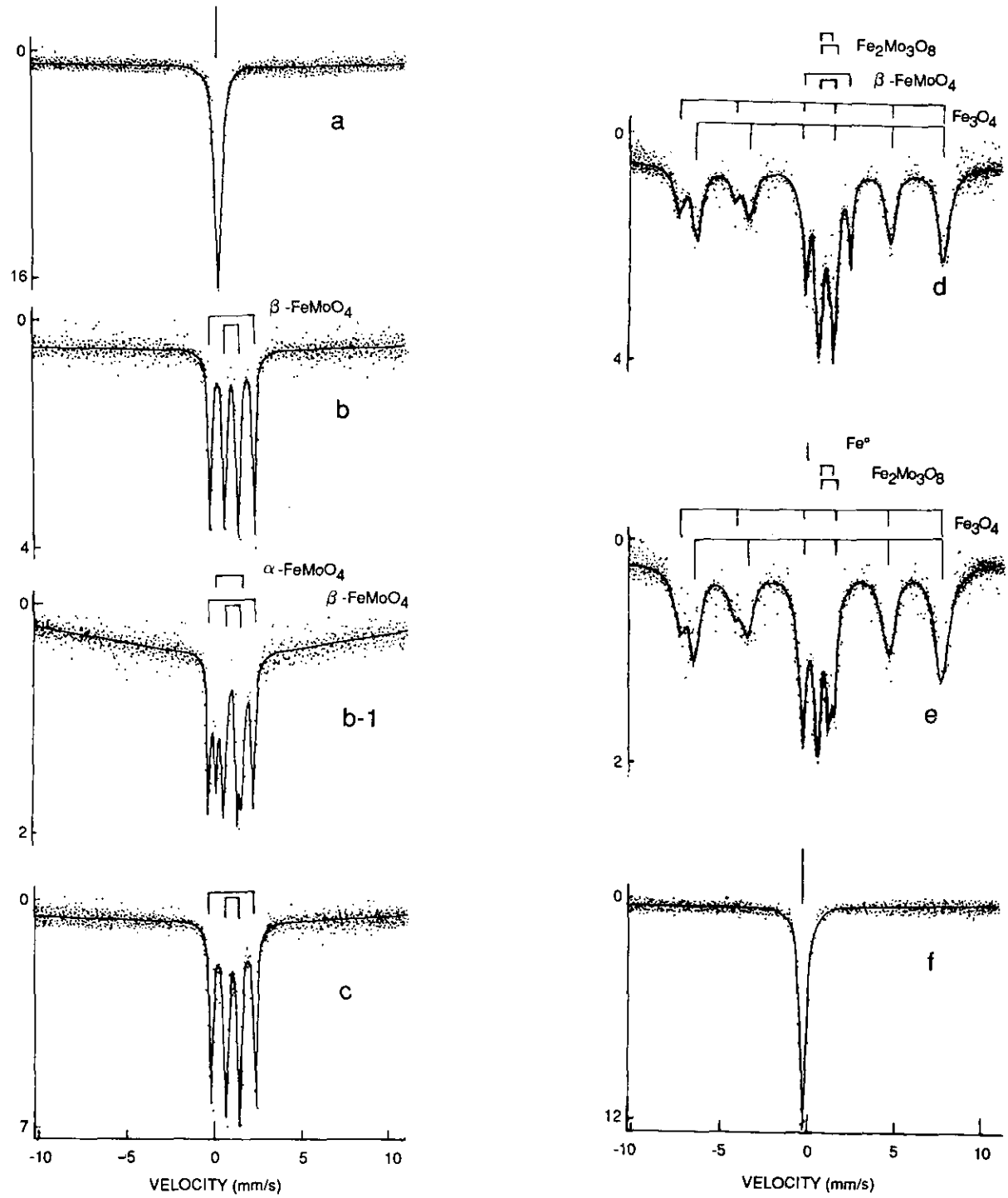

FIG. 3. *In situ* Mössbauer spectra for the Fe–Mo–O catalyst with an Fe/Mo atomic ratio of 0.29 recorded at different reduction stages: (a) before reduction; (b) after first TPR peak; (b–1) after first TPR peak and then exposed to air; and (c)–(f) after the second to fifth TPR peaks, respectively.

XRD measurements were performed in ambient atmosphere after the collection of Mössbauer spectra using the Rigaku D/Max-RA X-ray diffractometer equipped with a Cu target and graphite monochromator. The voltage and current employed were 30 kV and 50 mA, respectively.

RESULTS AND DISCUSSION

Figure 1 shows the TPR profiles of a series of Fe–Mo–O catalysts with different Fe/Mo atomic ratios. Two main reduction peaks at 968 and 1269 K can be observed in the

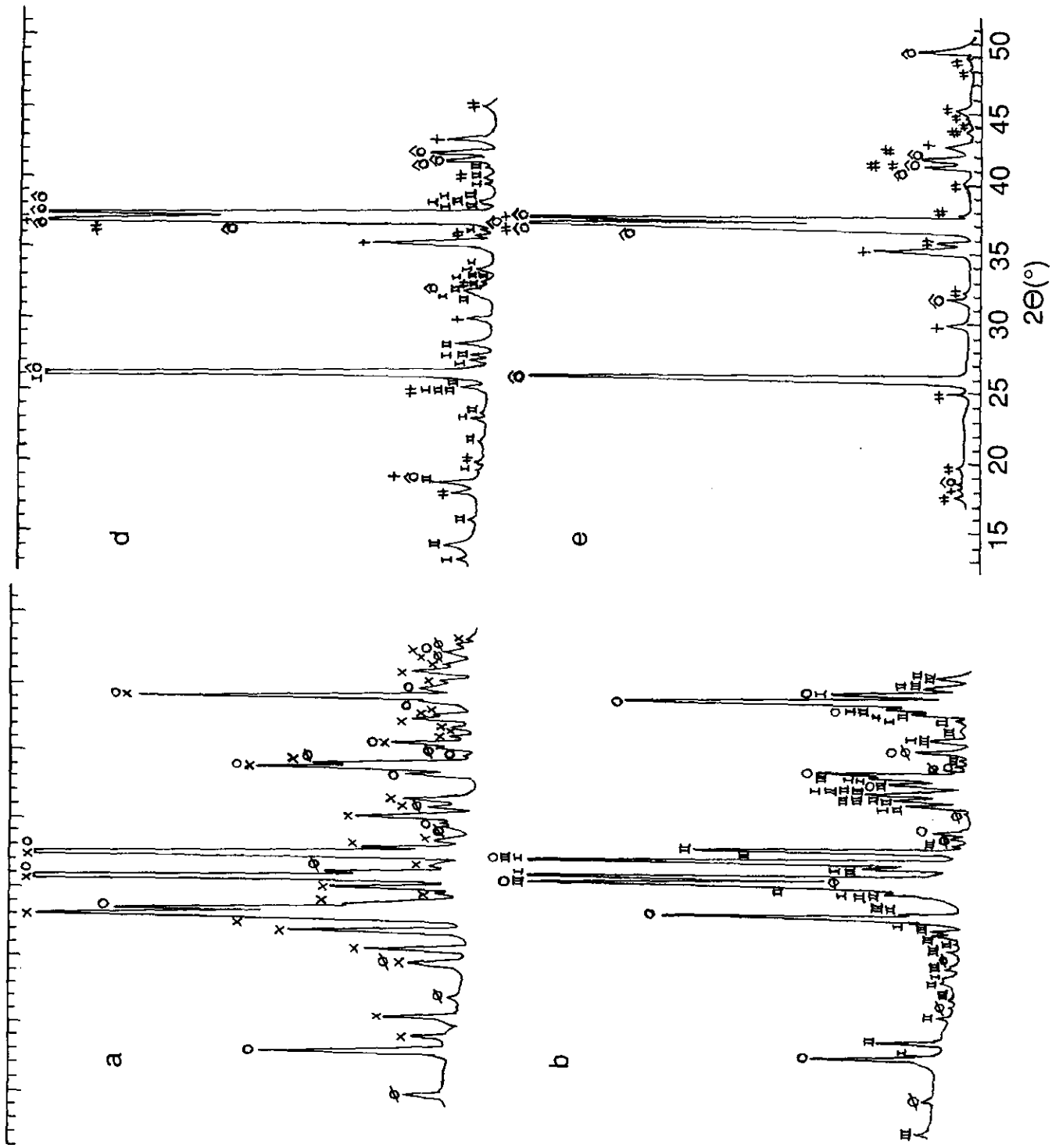
a
b
d
e
15
20
25
30
35
40
45
50
2Θ(°)

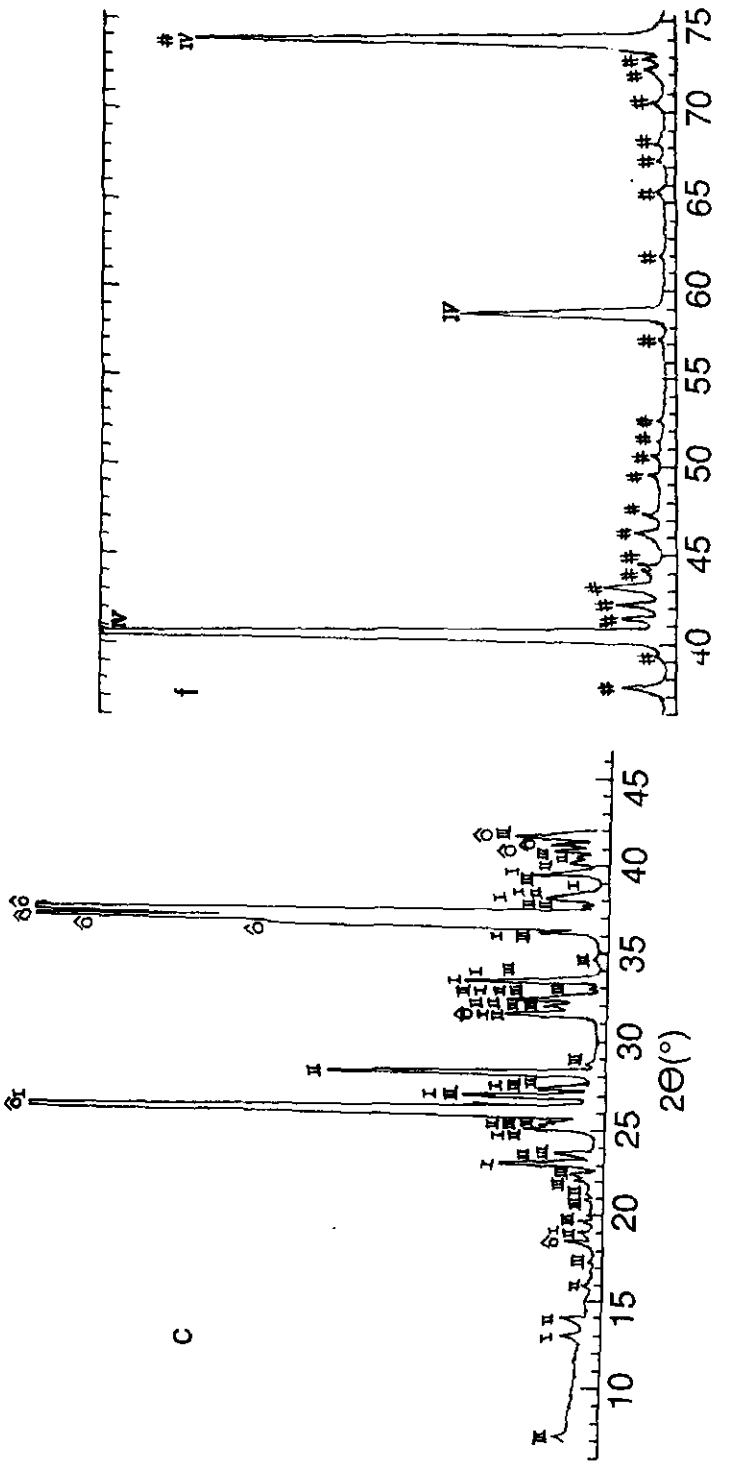

FIG. 4. XRD patterns of the Fe–Mo–O catalyst with an Fe/Mo atomic ratio of 0.29 measured in air following the determination of Mössbauer *spectroscopy*: (a) before reduction and (b)–(f) after the first to fifth TPR peaks, respectively. The symbols for the phases and the numbers of the JCPDS cards are (×) $Fe_2(MoO_4)_3$, 35–183 (31–642); (○) MoO_3, 5–508; (∅) MoO_3, 21–569; (I) β-$FeMoO_4$, 22–628; (II) α-$FeMoO_4$, 22–1115; (III) Mo_4O_{11}, 5–337; (δ) MoO_2, 32–671; (+) Fe_3O_4, 19–629; (++) $Fe_2Mo_3O_8$, 36–526; (#) Fe_3Mo, 31–641; and (IV) Mo^0, 4–809.

TABLE 1
Mössbauer Parameters of the Fe–Mo–O Catalyst with an Fe/Mo Atomic Ratio of 0.29 at Different TPR Stages

Peak in TPR	Peak temperature (K)	Mössbauer results				Peak area (%)	Assignment
		IS (mm/sec)	QS (mm/sec)	HF (kOe)	FWHM (mm/sec)		
Before reduction	RT	0.39	—	—	0.43	100	$Fe_2(MoO_4)_3$
First peak	853	1.12	0.82	—	0.25	50	β-$FeMoO_4$
		1.14	2.52	—	0.25	50	
First peak after XRD determination	853	1.12	0.81	—	0.27	37	β-$FeMoO_4$
		1.13	2.51	—	0.27	37	
		1.04	1.47	—	0.25	26	α-$FeMoO_4$
Second peak	910	1.12	0.80	—	0.29	51	β-$FeMoO_4$
		1.14	2.53	—	0.29	49	
Third peak	952	0.27	—	476	0.62	22	Fe_3O_4(T)
		0.62	—	433	0.62	38	Fe_3O_4(O)
		1.12	0.80	—	0.29	11	β-$FeMoO_4$
		1.14	2.53	—	0.29	11	
		0.90	0.58	—	0.35	9	$Fe_2Mo_3O_8$
		1.03	1.05	—	0.35	9	
Fourth peak	1014	0.29	—	472	0.74	27	Fe_3O_4(T)
		0.52	—	434	0.74	41	Fe_3O_4(O)
		0.90	0.58	—	0.35	11	$Fe_2Mo_3O_8$
		1.03	1.05	—	0.35	11	
		−0.21	—	—	0.45	10	Fe–Mo alloy
Fifth peak	1233	−0.21	—	—	0.45	100	Fe–Mo alloy

TPR profile of MoO_3 (Fig. 1a). According to the hydrogen consumption, the two TPR peaks are 33.8 and 66.2%; thus the area ratio for them is approximately 1 : 2, consistent with the two sequential reductions

$$MoO_3 + H_2 \rightarrow MoO_2 + H_2O \quad [1]$$

$$MoO_2 + 2H_2 \rightarrow Mo + 2H_2O. \quad [2]$$

Thus, the reduction of MoO_3 may proceed via two steps from Mo^{6+} to Mo^{4+} and then from Mo^{4+} to Mo^0. The small peak at 797 K and the shoulder peak at 918 K in the TPR profile of MoO_3 may be due to the formation of intermediate metastable phases, such as Mo_9O_{26} and Mo_8O_{23}, according to Arnoldy *et al.* (16).

For the Fe–Mo–O mixed oxides with an Fe/Mo atomic ratio of less than 0.67, the phases in the samples are MoO_3 and $Fe_2(MoO_4)_3$ (6, 7). From Fig. 1, it can be seen that with increased iron content (i.e., increased amount of $Fe_2(MoO_4)_3$ (6)), the temperatures of the two main TPR peaks decrease gradually. A small peak at 1023 K appears between the two main peaks, which may be attributed to the reduction of ferric ions since the peak does not appear in the TPR profile of MoO_3. In addition, the relative area of the TPR peak around 1233 K for Fe–Mo–O catalysts is about 70% of the total area of each profile, which is

TABLE 2
XRD Results of the Fe–Mo–O Catalyst with an Fe/Mo Atomic Ratio of 0.29 Obtained at Different TPR Reduction Stages

Peak	Peak temperature (K)	Phases detected by XRD
Before reduction	—	$Fe_2(MoO_4)_3$, MoO_3
First peak	853	MoO_3, α-$FeMoO_4$, β-$FeMoO_4$, Mo_4O_{11}
Second peak	910	MoO_2, α-$FeMoO_4$, β-$FeMoO_4$, Mo_4O_{11}
Third peak	952	MoO_2, Fe_3O_4, $Fe_2Mo_3O_8$, α-$FeMoO_4$, β-$FeMoO_4$
Fourth peak	1014	MoO_2, Fe_3O_4, $Fe_2Mo_3O_8$, Fe_3Mo (a little)
Fifth peak	1233	Mo^0, Fe_3Mo alloy

TABLE 3
The Possible Reactions that Take Place at Different TPR Peaks for the Fe–Mo–O Catalyst

Peak in TPR	Peak temperature (K)	Reactions
First	853	$4Fe_2(MoO_4)_3 + 5H_2 \rightarrow 8\beta\text{-}FeMoO_4 + Mo_4O_{11} + 5H_2O$
Second	910	$MoO_3 + H_2 \rightarrow MoO_2 + H_2O$
Third	952	$Mo_4O_{11} + 3H_2 \rightarrow 4MoO_2 + 3H_2O$
		$5\beta\text{-}FeMoO_4{}^a + 4H_2 \rightarrow Fe_3O_4 + Fe_2Mo_3O_8 + 2MoO_2 + 4H_2O$
Fourth	1014	$5\beta\text{-}FeMoO_4 + 4H_2 \rightarrow Fe_3O_4 + Fe_2Mo_3O_8 + 2MoO_2 + 4H_2O$
		$Fe_2Mo_3O_9{}^a + 2H_2 \rightarrow 2Fe + 3MoO_2 + 2H_2O$
		$MoO_2{}^a + 2H_2 \rightarrow Mo + 2H_2O$
		$Fe_3O_4{}^a + 4H_2 \rightarrow 3Fe + 4H_2O$
		$3Fe + Mo \rightarrow Fe_3Mo$ alloy
Fifth	1233	$Fe_2Mo_3O_8 + 2H_2 \rightarrow 2Fe + 3MoO_2 + 2H_2O$
		$Fe_3O_4 + 4H_2 \rightarrow 3Fe + 4H_2O$
		$MoO_2 + 2H_2 \rightarrow Mo + 2H_2O$
		$Mo + 3Fe \rightarrow Fe_3Mo$ alloy

[a] Only parts of these oxides participated in the reactions.

larger than 66.2% for MoO_3, indicating that some iron species may undergo reduction at this peak.

The TPR profiles as shown in Fig. 1 revealed that the reduction of Fe–Mo–O catalysts proceeds via several steps. To explain the phase changes at each reduction step, the sample with an Fe/Mo atomic ratio of 0.29 was examined in detail with *in situ* MBS and XRD after each TPR peak. Figure 2 shows the TPR profiles of the sample controlled at different reduction stages. Figures 3 and 4 show the Mössbauer spectra and XRD patterns collected after each TPR peak. The Mössbauer parameters and the phases detected by XRD are given in Tables 1 and 2, respectively.

As shown in Fig. 3a, the sample before reduction displayed a singlet in its Mössbauer spectrum (IS = 0.39 mm/sec), which can be assigned to ferric molybdate $Fe_2(MoO_4)_3$ (7, 10). The XRD results also revealed the existence of $Fe_2(MoO_4)_3$ as well as MoO_3.

After the first TPR peak at 853 K, the recorded Mössbauer spectrum showed a pattern with four absorption lines (Fig. 3b). This spectrum can be fitted with two doublets and can be assigned to β-$FeMoO_4$ following Sleight *et al.* (18). They reported two modifications of $FeMoO_4$, α-$FeMoO_4$ and β-$FeMoO_4$, at low pressure, and showed that the Mössbauer spectrum of α-$FeMoO_4$ displays one quadruple splitting transition with IS = 0.86 mm/sec and QS = 1.52 mm/sec. Bart *et al.* (17) also reported the formation of α-$FeMoO_4$ in Fe–Mo–O catalysts treated under N_2/CH_3OH at temperatures below 553 K. Surprisingly, the α-$FeMoO_4$ phase was not detected in our case by *in situ* Mössbauer spectroscopy after the first TPR peak. However, the subsequent XRD determination revealed α-$FeMoO_4$ as well as β-$FeMoO_4$, Mo_4O_{11}, and MoO_3 in the sample. The α-$FeMoO_4$ and β-$FeMoO_4$ phases detected by XRD exhibited their characteristic diffraction peaks at d = 3.164, 6.325, and 3.519 Å and at d = 3.403, 6.807, and 2.269 Å, respectively. Since the XRD measurements were performed after *in situ* Mössbauer determinations when the sample had been exposed to air, the α-$FeMoO_4$ might result from the phase transition of β-$FeMoO_4$ in ambient atmosphere. This was confirmed by reexamining the sample with Mössbauer spectroscopy after the XRD measurements. As shown in Fig. 3b-1, a doublet with IS = 1.04 mm/sec and QS = 1.47 mm/sec (see Table 1) belonging to α-$FeMoO_4$ was observed in addition to the two doublets for β-$FeMoO_4$ in the Mössbauer spectrum recorded after the sample was exposed to air.

Thus, both Mössbauer and XRD results revealed that $Fe_2(MoO_4)_3$ had been completely reduced at the first TPR peak. XRD results also showed that some Mo_4O_{11} was produced while the majority of MoO_3 was not affected. Furthermore, the reduction of MoO_3 to MoO_2 takes place at temperatures (968 K) much higher than 853 K. Based on these results, we attribute the first TPR peak at 853 K to the reduction of $Fe_2(MoO_4)_3$ as follows:

$$4Fe_2(MoO_4)_3 + 5H_2 \rightarrow 8\beta\text{-}FeMoO_4 + Mo_4O_{11} + 5H_2O. \quad [3]$$

The second reduction step is characteristic of the peak temperature at 910 K. The Mössbauer spectrum of the sample (Fig. 3c) recorded after this step is the same as that after the first TPR peak, indicating that β-$FeMoO_4$ was not affected. The subsequent XRD measurement revealed the phases of MoO_2, α-$FeMoO_4$, β-$FeMoO_4$, and Mo_4O_{11}. MoO_3 completely disappeared, while other phases remained after the second TPR peak. It is apparent

that the second TPR peak corresponds to the only reduction of MoO_3 to MoO_2 as expressed by Eq. [1]. It is interesting to note that the temperature for the reduction of MoO_3 to MoO_2 was lowered by the incorporation of iron.

Figure 3d shows the Mössbauer spectrum recorded for the sample after the third TPR peak at 952 K. This spectrum displays two sextuplets plus some doublets in the center. The sextuplets have the inner hyperfine fields of 476 and 433 kOe, respectively, characteristic of the parameters of Fe_3O_4. Two doublets belonging to β-$FeMoO_4$ can also be fitted. However, the subspectra of these two species cannot account for the whole spectrum. By subtracting the subspectra of Fe_3O_4 and β-$FeMoO_4$, two more doublets were fitted with parameters shown in Table 1, which may be assigned to $Fe_2Mo_3O_8$. The two doublets in the Mössbauer spectrum indicate two different environments for Fe^{2+} ions in $Fe_2Mo_3O_8$. In fact, Mo^{4+} ions are in octahedral sites and Fe^{2+} ions are in both octahedral and tetrahedral sites in $Fe_2Mo_3O_8$ (19). The formation of new species, Fe_3O_4 and $Fe_2Mo_3O_8$, at the third TPR peak was confirmed by XRD results (see Fig. 4d and Table 2). XRD also showed the disappearance of Mo_4O_{11} after the third TPR peak. Based on these results, two processes proceeding at the third TPR peak can be evaluated, i.e., the reduction of Mo_4O_{11} to MoO_2 and the transformation of part of the β-$FeMoO_4$ to Fe_3O_4 and $Fe_2Mo_3O_8$. These processes can be expressed as follows:

$$Mo_4O_{11} + 3H_2 \rightarrow 4MoO_2 + 3H_2O \quad [4]$$

$$5\beta\text{-}FeMoO_4 + 4H_2 \rightarrow Fe_3O_4 + Fe_2Mo_3O_8 + 2MoO_2 + 4H_2O. \quad [5]$$

At the first TPR peak, all iron ions have been reduced to Fe^{2+} in the form of β-$FeMoO_4$. However, at the third TPR peak, a great amount of Fe_3O_4 was produced, in which two-thirds of the iron ions are Fe^{3+}. Apparently, the reoxidation of Fe^{2+} to Fe^{3+} happened during the decomposition of β-$FeMoO_4$. In explaining this, let us consider the electrode potentials of the related iron and molybdenum species. Since the electrode potential of $\Phi^0_{Fe^{3+},Fe^{2+}}$ (0.771 V) (20) is much greater than that of $\Phi^0_{MoO_3,MoO_2,H^+}$ (0.320 V) (21), the reduction from Fe^{3+} to Fe^{2+} should be easier than that from Mo^{6+} to Mo^{4+}. This explains why only Fe^{3+} was reduced to Fe^{2+} (forming β-$FeMoO_4$) at the first TPR step. For the same reason, since $\Phi^0_{MoO_3,MoO_2,H^+}$ (0.320 V) is greater than $\Phi^0_{Fe^{2+},Fe^0}$ (−0.440 V) (20), Mo^{6+} will begin to reduce to Mo^{4+} when Fe^{3+} ions are completely reduced to Fe^{2+}. This is the case for the second TPR step. Again, since $\Phi^0_{MoO_3,MoO_2,H^+}$ (0.320 V) is greater than $\Phi^0_{Fe_3O_4,FeO,H^+}$ (−0.197 V) (21), it is possible for Mo^{6+} to reoxidize Fe^{2+} to Fe_3O_4. In fact, with the reoxidation of Fe^{2+} to Fe_3O_4, Mo^{6+} ions were reduced to Mo^{4+}, as expressed by Eq. [5].

After the fourth TPR peak at 1014 K, the Mössbauer and XRD results showed the disappearance of β-$FeMoO_4$ and the formation of the Fe–Mo alloy. At this step, β-$FeMoO_4$ was completely transformed to Fe_3O_4 and $Fe_2Mo_3O_8$. The Fe–Mo alloy that formed must result from the reduction of MoO_2 and Fe_3O_4 or $Fe_2Mo_3O_8$. Hence the fourth TPR peak corresponds to the reaction of Eq. [5] and the reductions of MoO_2 and Fe_3O_4 or $Fe_2Mo_3O_8$ to metals:

$$MoO_2 + 2H_2 \rightarrow Mo + 2H_2O \quad [6]$$

$$Fe_2Mo_3O_8 + 2H_2 \rightarrow 2Fe + 3MoO_2 + 2H_2O \quad [7]$$

$$Fe_3O_4 + 4H_2 \rightarrow 3Fe + 4H_2O. \quad [8]$$

The last TPR peak at 1233 K is about 70% of the total area of the TPR profile. At this step, all metal oxides were reduced to metals as expressed by Eqs. [6]–[8]. The products detected by Mössbauer spectroscopy and X-ray diffraction are Fe_3Mo alloy and metallic molybdenum. The Mössbauer spectrum of the Fe_3Mo alloy exhibits a singlet with an isomer shift of −0.21 mm/sec.

CONCLUSIONS

In summary, we have shown in this work that TPR combined with *in situ* Mössbauer spectroscopy and X-ray diffraction can provide useful information on the reduction process of metal oxides. For the Fe—Mo–O catalysts, the five TPR peaks corresponding to five different reduction steps have been clearly explained, and the reactions that take place at each step are summarized in Table 3. In addition, the transformation of ferrous molybdate from β-$FeMoO_4$ to α-$FeMoO_4$ under ambient atmosphere was confirmed. Finally, the Mössbauer spectrum of an intermediate reduction species, $Fe_2Mo_3O_8$, is reported.

ACKNOWLEDGMENTS

The authors acknowledge financial support from the Science Fund of Chinese Academy of Sciences and the Measurement Fund from the Modern Analysis Center of the Nanjing University. Jianyi Shen also acknowledges the financial support of Trans-Century Training Program Foundation for the Talents by the State Education Commission of China.

REFERENCES

1. N. Pernicone, *J. Less-Common Met.* **36,** 289 (1974).
2. B. C. Gates, J. R. Katzer, and G. C. A. Schuit, "Chemistry of Catalytic Processes," p. 328. McGraw–Hill, New York, 1979.
3. G. K. Boreskov, G. D. Kolovertnov, L. M. Kefeli, L. M. Playsova, L. G. Karakchiev, V. N. Mastikin, B. I. Popov, V. A. Dzinko, and D. V. Tarasova, *Kinet. Katal.* **7,** 144 (1966).
4. Y. Okamoto, F. Morikawa, K. Oh-Hiraki, T. Imanaka, and S. Teranishi, *J. Chem. Soc. Chem. Commun.*, 1018 (1981).

5. J. E. Germain and R. Laugier, *C.R. Acad. Sci. Ser. C.* **276,** 1349 (1973).
6. Hui-liang Zhang, Zong-chang Li, and Xian-cai Fu, *Cuihua Xuebao* **9,** 331 (1988).
7. Hui-liang Zhang, Zong-chang Li, Xian-cai Fu, Jian-Piang Huang, and Yu-chang Zhang, *J. Mol. Catal. (China),* **3,** 139 (1989).
8. D. Trifiro, V. De Vecchi, and I. Pasquon, *J. Catal.* **15,** 8 (1969).
9. M. Carbucicchio, and F. Trifiro, *J. Catal.* **45,** 77 (1976).
10. Hui-liang Zhang, Jian-yi Shen, and Xin Ge, *Hyperfine Interact.* **69**(1–4), 859 (1991).
11. P. L. Gai, and P. A. Labun, *J. Catal.* **94,** 79 (1985).
12. J. H. Wilson, III, C. G. Hill, Jr., and J. A. Dumesic, *J. Mol. Catal.* **61,** 333 (1990).
13. Hui-liang Zhang, Zong-chang Li, Xue-ying Zhao, and Xian-cai Fu, *Cuihua Xuebao* (*Chinese Journal of Catalysis*) **14**(2), 93 (1933).
14. Ren-yuan Tang, Rong-an Wu, and Li-wu Lin, *Appl. Catal.* **10,** 163 (1984).
15. Ren-yuan Tang, Su Zhang, Cheng-Yu Wang, Dong-bai Liang, and Li-wu Lin, *J. Catal.* **106,** 440 (1987).
16. P. Arnoldy, J. C. M. de Jonge, and J. A. Moulijn, *J. Phys. Chem.* **89,** 4517 (1985).
17. J. C. J. Bart, N. Burriesci, A. Gennaro, and M. Petrera, *Appl. Catal.* **7,** 151 (1983).
18. A. W. Sleight, B. L. Chamberland, and J. F. Weiher, *Inorg. Chem.* **7**(6), 1093 (1968).
19. Y. Le Page and P. Strobel, *Acta Crystallogr. Sect. B* **38,** 1265 (1982).
20. J. A. Dean (Ed.), "Lange's Handbook of Chemistry," 13th ed., p. 6–5. McGraw–Hill, New York 1972.
21. M. Pourbaix, "Atlas d'Equilibres Electro-Chimiques à 25 C," p. 272. Gauthier–Villars, Paris, 1963.